JACS
JOURNAL OF THE AMERICAN CHEMICAL SOCIETY

Article

pubs.acs.org/JACS

Visible Light-Induced Hole Injection into Rectifying Molecular Wires Anchored on Co_3O_4 and SiO_2 Nanoparticles

Han Sen Soo, Anil Agiral, Andreas Bachmeier,† and Heinz Frei*

Physical Biosciences Division, Lawrence Berkeley National Laboratory, University of California, Berkeley, California 94720, United States

Supporting Information

ABSTRACT: Tight control of charge transport from a visible light sensitizer to a metal oxide nanoparticle catalyst for water oxidation is a critical requirement for developing efficient artificial photosynthetic systems. By utilizing covalently anchored molecular wires for hole transport from sensitizer to the oxide surface, the challenge of high rate and unidirectionality of the charge flow can be addressed. Functionalized hole conducting molecular wires of type *p*-oligo(phenylenevinylene) (3 aryl units, abbreviated PV3) with various anchoring groups for the covalent attachment to Co_3O_4 catalyst nanoparticles were synthesized and two alternative methods for attachment to the oxide nanoparticle surface introduced. Covalent anchoring of intact PV3 molecules on Co_3O_4 nanoparticles (and on SiO_2 nanoparticles for control purposes) was established by FT-Raman, FT-IR, and optical spectroscopy including observation, in some cases, of the vibrational signature of the anchored functionality. Direct monitoring of the kinetics of hole transfer from a visible light sensitizer in aqueous solution ($[Ru(bpy)_3]^{2+}$ (and derivatives) light absorber, $[Co(NH_3)_5Cl]^{2+}$ acceptor) to wire molecules on inert SiO_2(12 nm) particles by nanosecond laser absorption spectroscopy revealed efficient, encounter controlled rates. For wire molecules anchored on Co_3O_4 nanoparticles, the recovery of the reduced sensitizer at 470 nm indicated similarly efficient hole transfer to the attached PV3, yet no transient hole signal was detected at 600 nm. This implies hole injection from the anchored wire molecule into the Co_3O_4 particle within 1 μs or shorter, indicating efficient charge transport from the visible light sensitizer to the oxide catalyst particle.

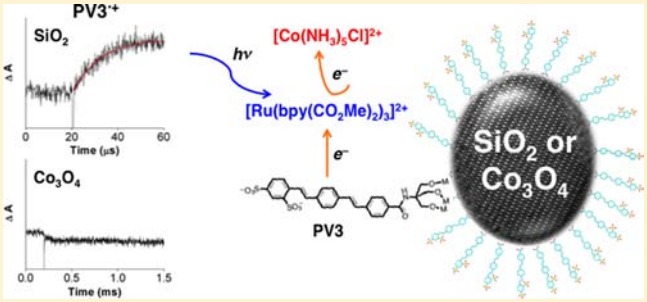

1. INTRODUCTION

For developing an efficient artificial photosynthetic system, a critical requirement is the delivery of charge from the light absorber to multielectron catalysts for water oxidation or fuel production with high quantum yield at low overpotential. Tight control of charge transport is favored for linkages that are molecularly defined and allow flow of electrons (or holes) only in the desired direction, while blocking transfer in the reverse sense. Such stringent control may be provided by molecular wires, especially the ones that impose directionality on the charge flow. We are exploring a method for coupling Co_3O_4 nanoparticles with a visible light chromophore through a hole conducting molecular wire embedded in a dense phase, few nanometers thin, silica shell that separates the catalyst from the chromophore. We have recently shown that the Co_3O_4 nanoparticles act as efficient multielectron catalysts for water oxidation at close to neutral pH.[1,2] Amorphous silica layers of nanometer depth are known to provide facile transport for protons while blocking passage of molecular products.[3] Using proper geometries, this approach could open up constructs for integrated systems that afford closure of the photosynthetic cycle on the nanoscale under separation of the water oxidation catalysis from the reduction chemistry. Spatial separation of the two chemistries by a product-impermeable layer is particularly important for the case of multistep CO_2 reduction, which may involve 4, 6, or even 8 electron transfer events. Moreover, coupling of a nanoparticulate water oxidation catalyst with the visible light chromophore by molecular wires might overcome the inefficient hole transfer between catalyst and light absorber commonly observed thus far for metal oxide catalysts.[4,5]

A class of well-established molecular wires for hole conduction are *p*-oligo(phenylenevinylene) molecules, which exhibit a very small rate dependence on distance for properly matched potentials of the attached components.[6,7] For the three membered representative 1,3-di((*E*)-styryl)benzene (abbreviated PV3, referring to 3 aryl units), the highest occupied molecular orbital (HOMO) has sufficient potential (E^0 = 1.32 V vs SHE)[7,8] to drive a Co_3O_4 nanoparticle catalyst for water oxidation. At the same time, hole injection into this wire molecule is energetically accessible by mild donors such as Ru bipyridyl-type visible light sensitizers.[9] With the PV3 LUMO situated at −1.7 V (vs SHE), electrons from the visible light-excited sensitizer cannot be accepted by the wire, thus, imposing unidirectional charge flow. Efficient transfer of charge from wire molecules to the nanoparticle catalyst may require

Received: July 2, 2012
Published: August 30, 2012

dx.doi.org/10.1021/ja306162g | J. Am. Chem. Soc. 2012, 134, 17104−17116

covalent anchoring on the metal oxide surface. While covalent charge transport linkers to Co oxide surfaces have not been explored so far to our knowledge, functionalities such as carboxylate, phosphonate, ether, or acetyl acetonate commonly used for anchoring of visible light sensitizers on TiO_2 in dye sensitized solar cells offer a starting point.[4,10−14] Moreover, photochemical grafting of terminal vinyl groups results in stable attachment to TiO_2 surfaces as well.[15] For achieving orientation of the wire molecules vertical to the nanoparticle surface, polydentate and tripodal anchors with terminal OH groups are of particular interest.[11,16−20]

In this paper, we report on the synthesis, characterization, and attachment of molecular wires on Co_3O_4 catalyst surfaces, and on the demonstration of visible light-sensitized hole transfer to the anchored wire molecules. The syntheses and characterization of 1,3-di((*E*)-styryl)benzene molecules featuring several different functionalities for covalent anchoring on oxide nanoparticle surfaces are presented. Optical, FT-infrared, and FT-Raman spectroscopy are employed for monitoring covalent attachment to the oxide particle surface. Transient optical measurements on the nano- and microsecond time scale provide direct evidence for efficient hole injection from a Ru bipyridyl-type visible light sensitizer into molecular wires anchored on Co_3O_4 and SiO_2 nanoparticles. Embedding of the anchored wire molecules into an amorphous, nanoscale silica layer, and core−shell constructs with proper geometry (e.g., nanotubes) for the development of an integrated system that affords water oxidation catalysis separated from chromophore and reduction chemistry will be reported in forthcoming papers.

2. RESULTS

2.1. Design, Synthesis, and Characterization of *p*-Oligo(phenylenevinylene) Molecular Wires. The PV3 derivatives were assembled by the *trans*-selective Wittig−Horner reaction[21−23] after incorporating the desired hydrophilic[24] and anchoring functional groups in the precursors. A perpendicular (radial) orientation of the molecular wires with respect to the oxide particle surface is required in order to achieve spatial separation of the water oxidation from chromophore/carbon dioxide reduction catalytic sites by a few nm and minimize through-space back charge transfer. Furthermore, radial orientation prevents aggregation and intermolecular $\pi-\pi$ interactions, thus will enable subsequent casting of a gas separating but proton-conducting silica layer around the wire molecules (schematically shown in Figure 1). To minimize perturbation of the electronic structure of the conjugated π-electron system, the anchoring groups for the molecular wires were introduced only at the *para* position of one terminal benzene ring of the PV3 molecules. For the PV3 molecules to be water-soluble, sulfonate groups were incorporated into the benzene ring at the other end of the PV3 molecular wires.[22] In addition to facilitating water solubility, sulfonate groups are poor conjugate bases and nucleophiles, and therefore unlikely to covalently attach to metal oxide surfaces, which might otherwise result in cross-linking and aggregation of the functionalized nanoparticles.

For the determination of hole injection efficiency from a visible light sensitizer into wire molecules in homogeneous aqueous solution, the water-soluble sodium 2,2′-((1*E*,1′*E*)-1,4-phenylenebis(ethene-2,1-diyl))dibenzenesulfonate (**Na_2PV3_SO3_SO3**) was prepared in good yields by a straightforward one-step Wittig−Horner reaction between

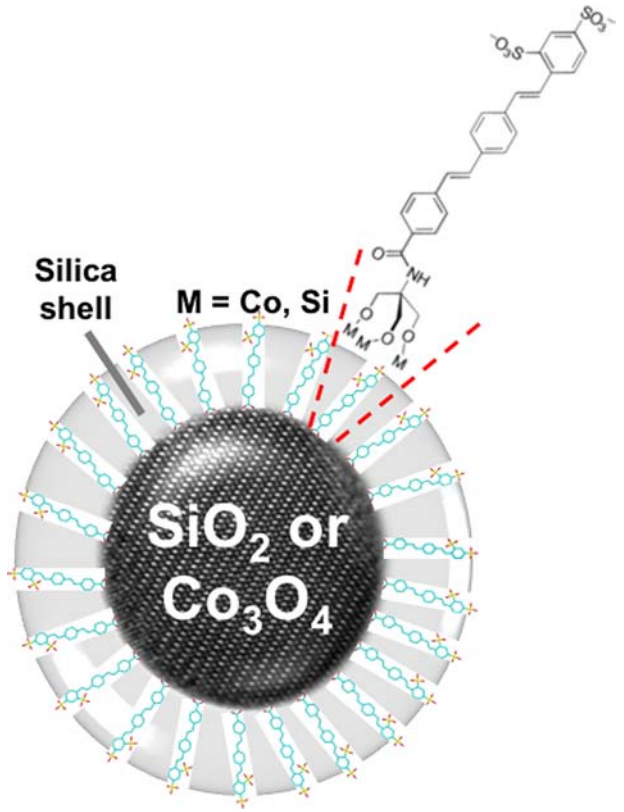

Figure 1. Core−shell construct with tripodally anchored, hole-conducting PV3 molecular diodes embedded in a proton-conducting silica shell.

sodium 2-formylbenzenesulfonate (**1**) and tetraethyl (1,4-phenylenebis(methylene))bis(phosphonate) (**2**) (Scheme 1).

Asymmetrically functionalized oligo(phenylenevinylene) wires were synthesized in a convergent and modular fashion. The routes to the mono *para*-sulfonated PV3 oligomer ethyl 4-((*E*)-4-((*E*)-4-cyanostyryl)styryl)benzenesulfonate (**PV3_CN_SO2OEt**) and its more hydrophilic derivatives are illustrated in Schemes 2 and 3. The nitrile precursor (*E*)-4-(4-(diethoxymethyl)styryl)benzonitrile (**PV2_CN_CH(OEt)2**) is isolated with high *trans* regioselectivity and high yields from the Wittig−Horner reaction between 4-(diethoxymethyl)-benzaldehyde (**3**) and diethyl 4-cyanobenzylphosphonate (**4**). The nitrile group is versatile and can be readily transformed into anchors such as carboxylates, aldehydes, alcohols, amines, or further converted into chelating groups. The acetal can be hydrolyzed under mild acidic conditions with aqueous acetic acid in a biphasic reaction to provide (*E*)-4-(4-formylstyryl)-benzonitrile (**PV2_CN_C(O)H**), with another formyl group for a subsequent Wittig−Horner reaction with an appropriately derivatized hydrophilic aryl phosphonate. Methyl 4-(bromomethyl)benzenesulfonate (**5**) is converted via the Arbuzov reaction with triethyl phosphite (**6**) into ethyl 4-((diethoxyphosphoryl)methyl)benzenesulfonate (**7**) in quantitative yields.[22] Subsequent reaction between **PV2_CN_C(O)H** and **7** in the presence of a strong base gave **PV3_CN_SO2-(OEt)** as a yellow solid in good yields without the need for column chromatography in this entire reaction sequence.

Attempts at basic hydrolysis of **PV3_CN_SO2(OEt)** with aqueous NaOH or KOH yielded a yellow solid material that is poorly soluble in water. Hydrolysis at elevated temperatures and pressures in an autoclave with CsOH produced cesium 4-

dx.doi.org/10.1021/ja306162g | J. Am. Chem. Soc. 2012, 134, 17104−17116

Scheme 1. Preparation of the Water-Soluble Na_2PV3_SO3_SO3 by the Wittig–Horner Reaction

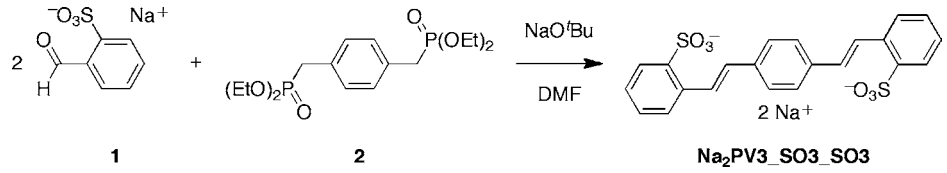

Scheme 2. Convergent Synthesis of PV3_CN_SO2(OEt)

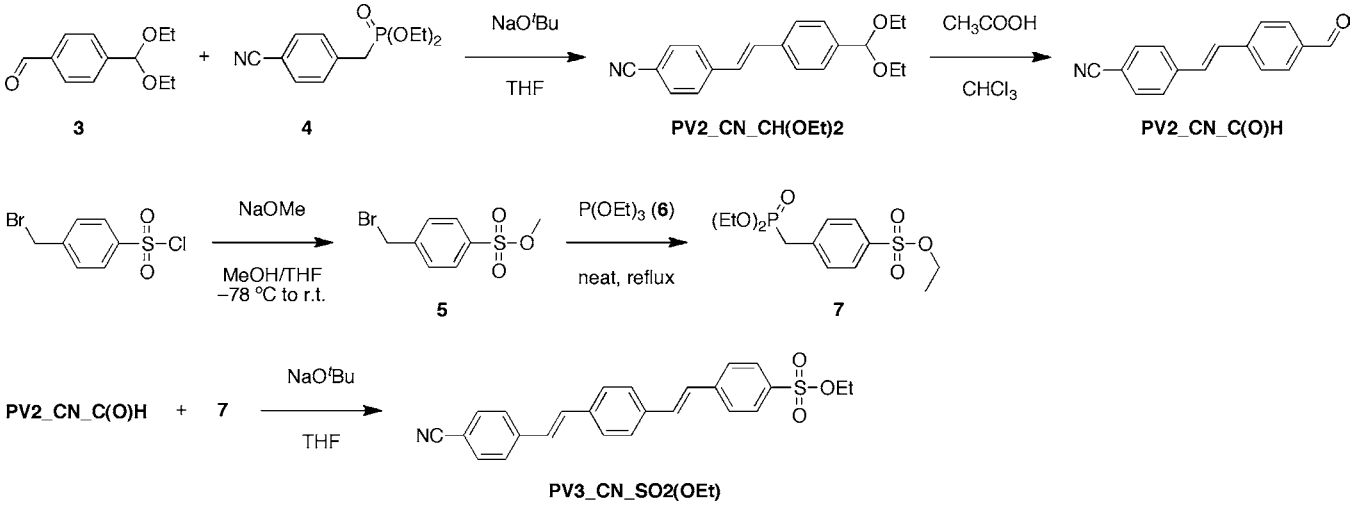

Scheme 3. Hydrophilic Functionalization of PV3_CN_SO2(OEt) by Hydrolysis and Conversion into an Amide

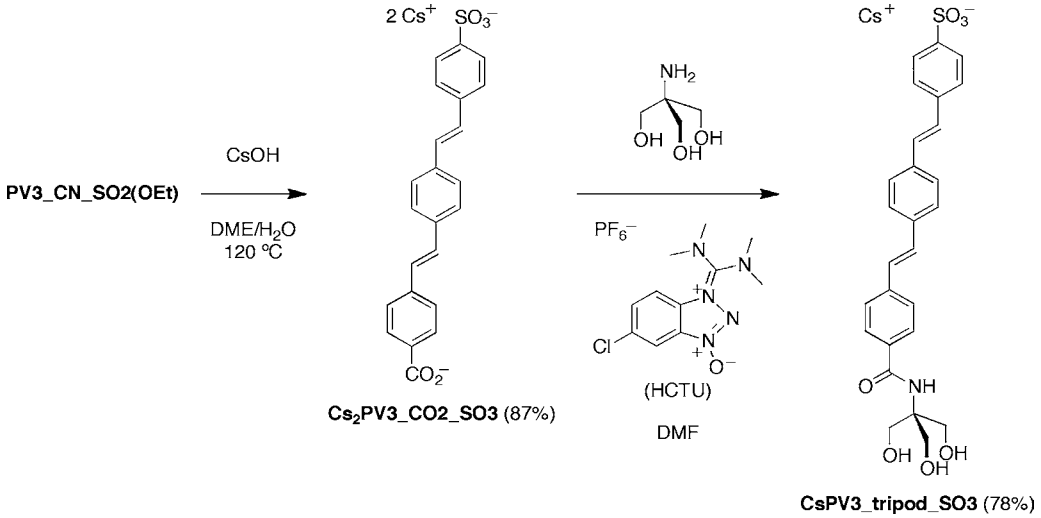

((*E*)-4-((*E*)-4-sulfonatostyryl)styryl)benzoate (**Cs_2PV3_CO2_SO3**, Scheme 3), which is still only sparingly soluble in water and dimethyl sulfoxide (DMSO), but sufficient amounts dissolved for characterization by ^{1}H NMR spectroscopy. In accordance to observations in previous studies,[22] *para*-sulfonated PV3 molecules have poor solubility in water, presumably due to the hydrophobic π-stacking interactions. In an attempt to disrupt the strong intermolecular forces of the PV3 molecules and install three anchor points in a tripodal perpendicular arrangement for the molecular wires on metal oxide surfaces, **Cs_2PV3_CO2_SO3** is condensed with tris(hydroxymethyl)aminomethane (**8**) using *O*-(6-chlorobenzotriazol-1-yl)-*N*,*N*,*N*′,*N*′-tetramethyluronium hexafluorophosphate (HCTU) as the peptide coupling agent.[25,26] However, the isolated yellow cesium 4-((*E*)-4-((*E*)-4-((1,3-dihydroxy-2-(hydroxymethyl)propan-2-yl)carbamoyl)-styryl)styryl)-benzenesulfonate (**CsPV3_tripod_SO3**) has only slightly enhanced aqueous solubility, prompting further synthetic modifications to the hydrophilic component for coupling with **PV2_CN_C(O)H**.

On the basis of the reasonable water solubility of **Na_2PV3_SO3_SO3**, we surmised that *ortho* substitution on PV3 molecules may minimize the π-stacking interactions. The derivative **Cs_3PV3_CO2_2SO3** was thus designed with this insight in mind and the assembly is presented in Scheme 4. Hydrogenation of sodium 4-formylbenzene-1,3-disulfonate (**9**) with NP Pd(0)EnCat 30[27] as the catalyst provides sodium 4-(hydroxymethyl)benzene-1,3-disulfonate (**10**) in good yields without need for further purification. The use of 10% Pd/C with various additives such as ethylenediamine[28] in different

dx.doi.org/10.1021/ja306162g | J. Am. Chem. Soc. 2012, 134, 17104–17116

Scheme 4. Convergent Preparative Route to the Water-Soluble Cs_3PV3_CO2_2SO3

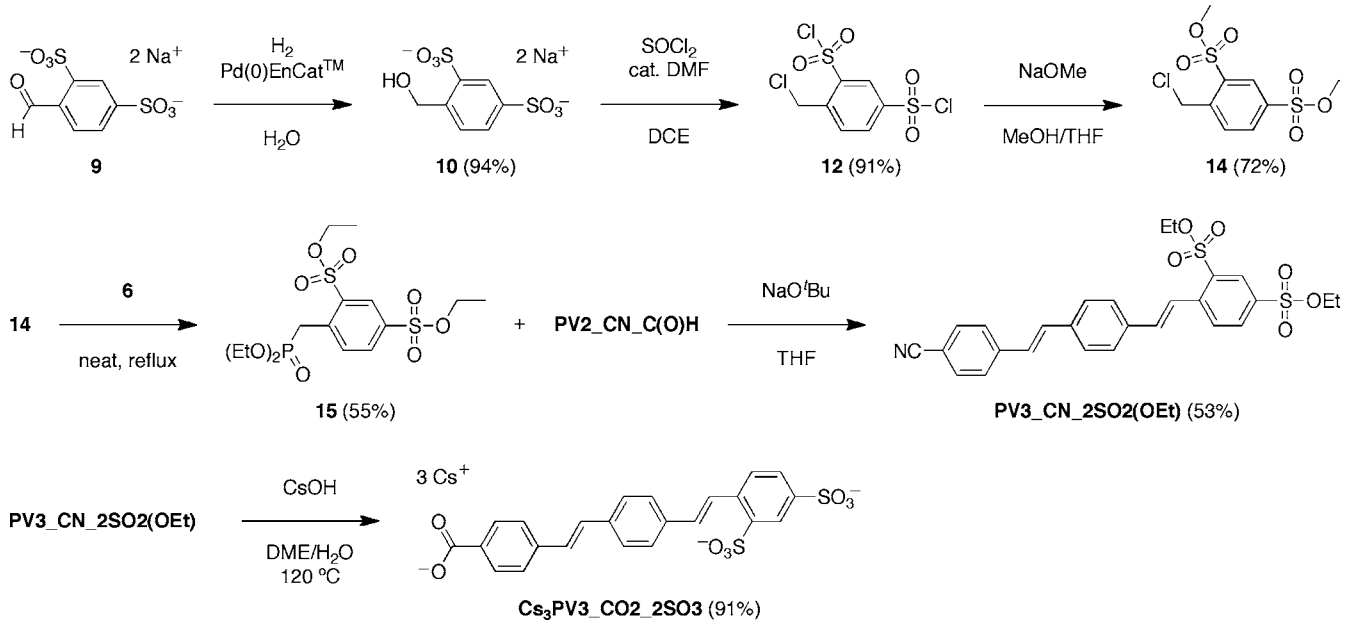

Scheme 5. Transformation of Cs_3PV3_CO2_2SO3 into Chelating, Poly-ol Anchors by Amide Coupling

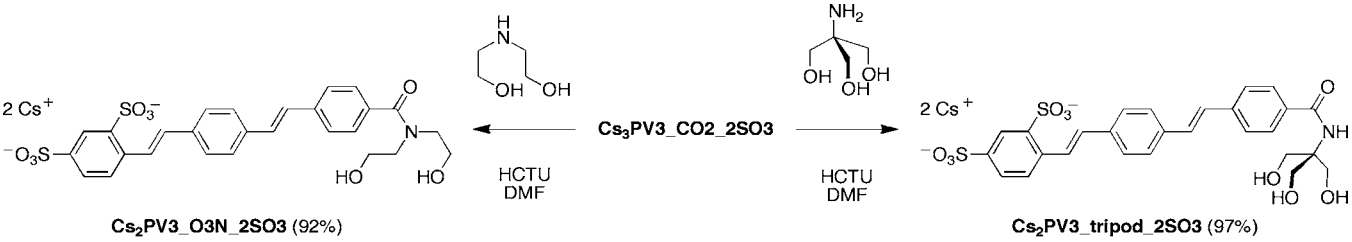

solvents invariably leads to a mixture of unreacted starting material, product, and the over-reduced byproduct 4-methylbenzene-1,3-disulfonate (**11**), which cannot be readily separated without reverse-phase column chromatography. Chlorination of finely crushed **10** with $SOCl_2$ and catalytic amounts of *N*,*N*-dimethylformamide (DMF) to produce 4-(chloromethyl)-benzene-1,3-disulfonyl chloride (**12**),[29] followed by methylation using sodium methoxide (**13**), yields dimethyl 4-(chloromethyl)benzene-1,3-disulfonate (**14**) as a viscous, orange oil.[30,31] Subsequent Arbuzov reaction[22] between **6** and **14** led to an unexpectedly complex mixture, from which diethyl 4-((diethoxyphosphoryl)methyl)benzene-1,3-disulfonate (**15**) is isolated as a colorless oil after purification by column chromatography on silica. A Wittig–Horner reaction between **PV2_CN_C(O)H** and **15** also resulted in a mixture of products, and diethyl 4-((*E*)-4-((*E*)-4-cyanostyryl)styryl)-benzene-1,3-disulfonate (**PV3_CN_2SO2(OEt)**) was purified by silica column chromatography and collected in moderate yields. Hydrolysis of **PV3_CN_2SO2(OEt)** at elevated temperatures and pressures in an autoclave with a concentrated aqueous solution of CsOH produced cesium 4-((*E*)-4-((*E*)-2,4-disulfonatostyryl)styryl)benzoate (**Cs_3PV3_CO2_2SO3**). The compound is readily soluble in water and somewhat soluble in methanol.

To achieve covalent attachment to metal oxide surfaces (vide infra), the two derivatives cesium 4-((*E*)-4-((*E*)-4-(bis(2-hydroxyethyl)carbamoyl)styryl)styryl)benzene-1,3-disulfonate (**Cs_2PV3_O3N_2SO3**) and cesium 4-((*E*)-4-((*E*)-4-((1,3-dihydroxy-2-(hydroxymethyl)propan-2-yl)carbamoyl)-styryl)-styryl)benzene-1,3-disulfonate (**Cs_3PV3_tripod_2SO3**) were synthesized. These congeners have two and three alcohol groups for condensation with surface M–OH (M = Si, Co) groups, and were prepared in similar fashion to the monosulfonated version above with HCTU as the dehydrating agent (Scheme 5).[25,26] All precursors were characterized by ^{1}H and ^{13}C NMR spectroscopy and high resolution mass spectrometry. In addition, the PV2 and PV3 oligomers were further studied using FT-IR, FT-Raman, and UV–visible spectroscopy because these techniques offer unique features of the molecules that are essential for verifying the covalent anchoring of the PV3 molecular wires on the metal oxide surfaces.

2.2. Transient Absorption Spectroscopy of Hole Injection into Free Molecular Wires in Aqueous Solution. The ground state optical absorption spectra of representative examples of the PV2 and PV3 molecular wires measured in chloroform or in water are displayed in Figure 2, while the absorption maxima (λ_{max}) and extinction coefficients (ε) are summarized in Table 1. All spectra exhibit at least one intense absorption band between 320 and 380 nm, with extinction coefficients equal or exceeding 29 000 M^{-1} cm^{-1}, attributable to an aromatic $\pi-\pi^*$ transition.[32] The observed red shift of the $\pi-\pi^*$ band from **PV2_CN_C(O)H** to **PV3_CN_2SO2(OEt)** is consistent with the extended conjugation of the PV3 congeners compared to the PV2 precursors. The absence of a substantial solvent shift of the PV3

dx.doi.org/10.1021/ja306162g | J. Am. Chem. Soc. 2012, 134, 17104–17116

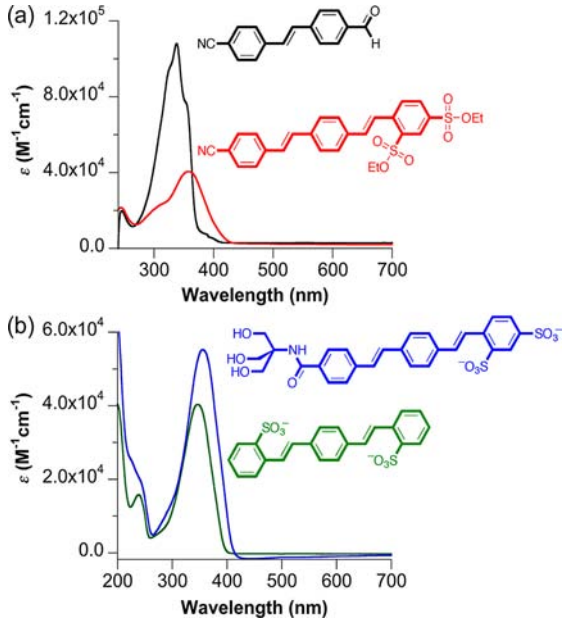

Figure 2. (a) UV−visible spectra of 10 μM **PV2_CN_C(O)H** (black) and 25 μM **PV3_CN_2SO2(OEt)** (red) in $CHCl_3$. (b) UV−visible spectra of 12.5 μM **Cs_2PV3_tripod_2SO3** (blue) and 25 μM **Na_2PV3_SO3_SO3** (green) in water. All spectra were collected in 10 × 5 mm cuvettes.

Table 1. Photophysical Properties of New PV2 and PV3 Oligomers in Solution[a]

oligomer	λ_{max} (nm)	ε (10^4 $M^{-1}cm^{-1}$)
PV2_CN_CH(OEt)2	327	6.09
PV2_CN_C(O)H	241	2.29
	325	9.29
	354	7.52
PV3_CN_SO2(OEt)	244	2.31
	371	6.09
PV3_CN_2SO2(OEt)	243	1.73
	356	3.68
Na_2PV3_SO3_SO3	239	1.49
	349	4.14
Cs_2PV3_CO2_SO3	242	1.80
	306	1.90
	361	2.92
CsPV3_tripod_SO3	250	2.51
	323	3.72
	405[b]	0.99
Cs_3PV3_CO2_2SO3	242	1.53
	363	5.05
Cs_2PV3_O3N_2SO3	241	3.53
	361	7.95
Cs_2PV3_tripod_2SO3	243	2.09
	356	5.38

[a]Ionic compounds in aqueous solution, and neutral organic molecules in $CHCl_3$. [b]Shoulder.

π−π* peak between chloroform and water indicates that, in dilute solution, species in both solvents are well dispersed and do not undergo aggregation by π-stacking. Therefore, we do not expect excited state−excited state annihilation processes to play a role in dilute solutions.[33,34]

Transient absorption measurements were conducted to probe for spectral signatures of hole injection into PV3 molecules in aqueous solution. The transient optical experiments were carried out with $[Ru(bpy)_3]^{2+}$ or $[Ru(bpy(CO_2Me)_2)_3]^{2+}$ (bpy = 2,2′-bipyridine; $bpy(CO_2Me)_2$ = 2,2′-bipyridine-4,4′-dimethylcarboxylate) as the visible light sensitizers and $Na_2S_2O_8$ or $Co(NH_3)_5Cl_3$ as the sacrificial electron acceptor. These are established visible light sensitization systems[35] in which a Ru^{III} complex is generated at a potential suitable for hole injection into the wire molecules. The energetics and kinetics of the electron transfer processes leading to the oxidized Ru complex have been reported.[7,36] The standard redox potentials of these reagents and PV3 (1,3-di((*E*)-styryl)benzene) are listed in Table 2 (relative to NHE in aqueous solution).[7,21,38−45] The energetics of the Ru complexes and the parent PV3 molecule confirm that the metal-to-ligand charge transfer (MLCT) excited state $[Ru(bpy)_3]^{2+*}$ does not have sufficient potential to oxidize or reduce PV3 molecules.[38] The only process that may occur in the absence of an electron acceptor for quenching of the excited Ru complex is triplet−triplet energy transfer from $[Ru(bpy(CO_2Me)_2)_3]^{2+*}$ to **Na_2PV3_SO3_SO3**. The lifetime of the excited ^{3}PV3 molecules so formed was found to be 1.39 ± 0.02 μs in aqueous solutions (Supporting Information Figure S1). Upon quenching with a sacrificial electron acceptor $S_2O_8^{2-}$ or $Co(NH_3)_5Cl^{2+}$, oxidized sensitizers $[Ru(bpy)_3]^{3+}$ or $[Ru(bpy(CO_2Me)_2)_3]^{3+}$so formed have sufficient potential to oxidize PV3 molecules (unfunctionalized). On the other hand, reduction of PV3 by the excited sensitizer is thermodynamically not possible (Table 2 and Figure 3). The parent $[Ru(bpy)_3]^{3+}$ sensitizer only has a modest overpotential available to oxidize unfunctionalized PV3 molecules. Since all PV3 derivatives investigated in this work have electron-withdrawing groups such as sulfonates, carboxylates, and amides, the required potential for oxidation is expected to be more positive than that for unfunctionalized PV3. For this reason, $[Ru(bpy(CO_2Me)_2)_3]^{2+}$ was used as the standard chromophore in the time-resolved experiments.

Table 2. Reduction Potentials of Reagents Used in Time-Resolved Spectroscopic Studies

reagent	$E_{1/2}$ (V)[a]
$PV3^+/PV3$[b]	1.32[7,41]
$PV3/PV3^-$[b]	−1.69[7,41]
$Ru(bpy)_3^{3+}/ Ru(bpy)_3^{2+}$	1.45[39−41]
$Ru(bpy)_3^{2+}/ Ru(bpy)_3^{+}$	−1.17[39−41]
$Ru(bpy)_3^{2+*}/ Ru(bpy)_3^{+}$	0.84[39−41]
$Ru(bpy)_3^{3+}/ Ru(bpy)_3^{2+*}$	−0.84[39−41]
$Ru(bpy[CO_2Me])_3^{3+}/ Ru(bpy[CO_2Me])_3^{2+}$[c]	1.80[41,42]
$Ru(bpy[CO_2Me])_3^{2+}/ Ru(bpy[CO_2Me])_3^{+}$[c]	−0.66[41,42]
$S_2O_8^{2-}/SO_4^{-*}$	1.96[44,45]
SO_4^{-*}/SO_4^{2-}	2.43[44,45]
$Co(NH_3)_5Cl^{2+}/Co^{2+}$	0.33[43]
O_2/H_2O	1.23[44,45]

[a]Potentials relative to standard hydrogen electrode in water unless otherwise noted. [b]The potentials were measured in butyronitrile with the sodium calomel reference electrode[7] and the value reported here has been corrected to SHE in aqueous solutions.[41] [c]The potentials were measured in acetonitrile with ferrocene as the internal standard[42] and the value reported here has been corrected to SHE in aqueous solutions.[41]

For typical nanosecond pump−probe measurements, samples purged with N_2 in quartz cuvettes beforehand were

dx.doi.org/10.1021/ja306162g | J. Am. Chem. Soc. 2012, 134, 17104−17116

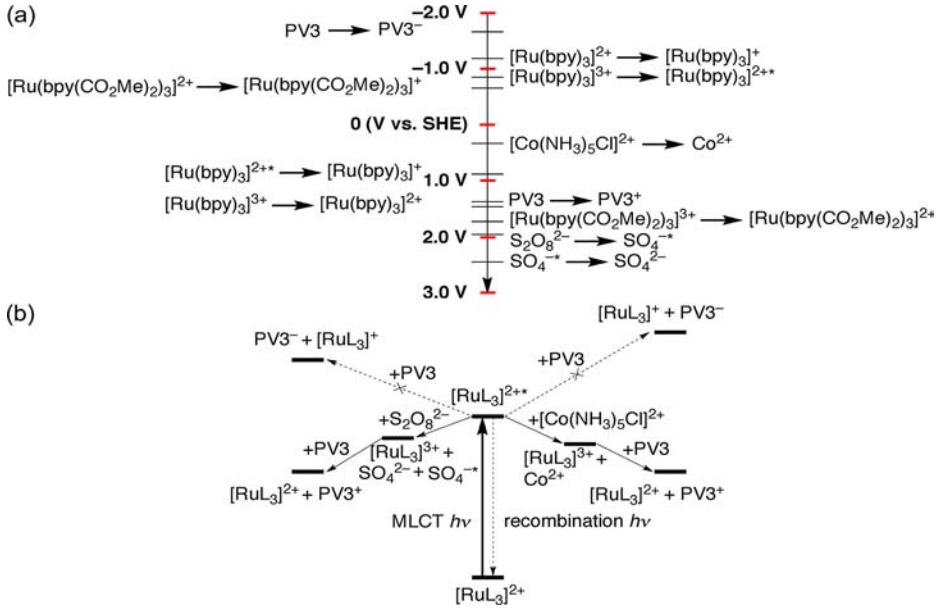

Figure 3. (a) Redox potential (vs SHE) diagram of the reagents used in time-resolved optical spectroscopy; the detailed potentials are summarized in Table 2. (b) Plausible reaction paths (solid arrows) and thermodynamically unfavorable reactions (dashed arrow with cross) in pump−probe measurements with PV3 wires.

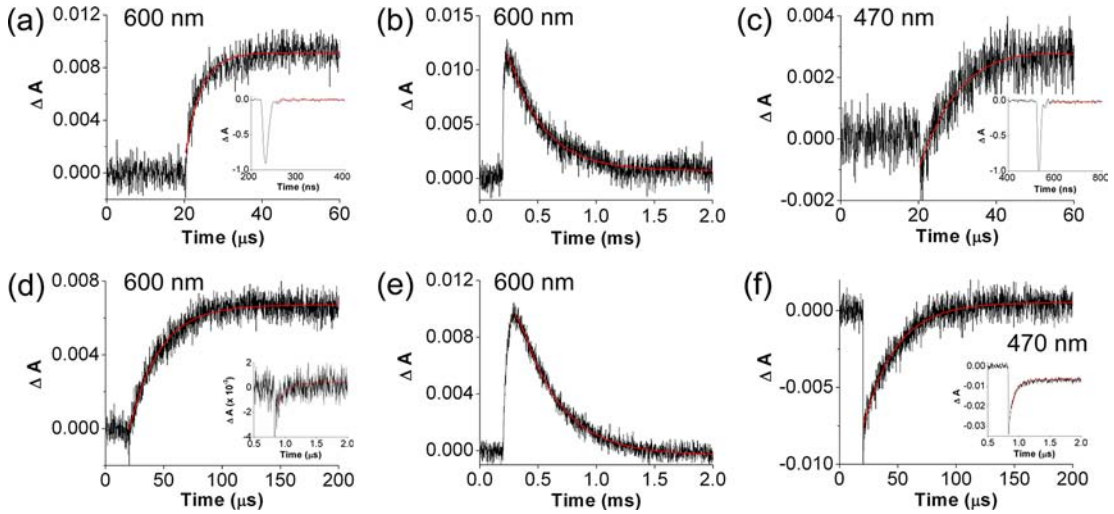

Figure 4. (a) Transient absorption signal at 600 nm upon 450 nm excitation of sensitizer in the presence of **Na_2PV3_SO3_SO3** (0.26 mM)($S_2O_8^{2-}$, 0.50 M; $[Ru(bpy(CO_2Me)_2)_3]^{2+}$, 5 μM). Inset: phosphorescence recovery at 600 nm on expanded time scale. (b) Decay of $PV3^+$ 600 nm signal. (c) Bleach recovery of $[Ru(bpy(CO_2Me)_2)_3]^{2+}$ and growth of $PV3^+$ at 470 nm. Inset: bleach recovery at 470 nm on expanded scale. (d) Transient absorption signal at 600 nm upon 450 nm excitation of sensitizer in the presence of **Cs_2PV3_O3N_2SO3** (50 μM)($Co(NH_3)_5Cl^{2+}$, 10 mM; $[Ru(bpy(CO_2Me))_3]^{2+}$, 10 μM). Inset: Phosphorescence recovery at 600 nm on expanded scale. (e) Decay of $PV3^+$ 600 nm signal. (f) Bleach recovery of $[Ru(bpy(CO_2Me)_2)_3]^{2+}$ at 470 nm. Inset: Bleach recovery at 470 nm on expanded scale.

illuminated at 450 nm (3−8 mJ/pulse, 8 ns pulse duration) to excite the MLCT transition of $[Ru(bpy(CO_2Me)_2)_3]^{2+}$, a wavelength that avoids direct excitation of the PV3 molecules. A large excess (0.5 M, 2×10^4 to 10^5 equivalents) of $S_2O_8^{2-}$ relative to $[Ru(bpy(CO_2Me)_2)_3]^{2+}$ was used to ensure formation of substantial concentrations of $[Ru(bpy(CO_2Me)_2)_3]^{3+}$. In time-resolved measurements with excess **Na_2PV3_SO3_SO3** relative to $[Ru(bpy(CO_2Me)_2)_3]^{2+}$, the reaction was probed at 470 nm near the MLCT λ_{max} of the sensitizer, and at 600 nm where the absorption λ_{max} of PV3 radical cations is anticipated (Figure 4).[7] The radical cation absorption at 600 nm overlaps with the phosphorescence of $[Ru(bpy(CO_2Me)_2)_3]^{2+}$. As shown in Figure 4c, at 470 nm, the recovery of the ground state from the sensitizer photobleach, shown on an expanded scale in the inset, is followed by growth of the PV3 radical absorption. By contrast, only partial recovery of the photobleach of $[Ru(bpy(CO_2Me)_2)_3]^{2+}$ is observed in the absence of **Na_2PV3_SO3_SO3** (Supporting Information Figure S2a). When probed at 600 nm (Figure 4a), the rise time of the PV3 radical absorption is 4.5 ± 0.2 μs (preceded on the nanosecond time-scale by $[Ru(bpy(CO_2Me)_2)_3]^{2+}$ phosphorescence decay shown in the inset), in agreement with the bleach recovery at 470 nm (4.9 ± 0.1 μs). The 600 nm $PV3^+$ absorption signal decays slowly with a time constant of 300 ± 5 μs (Figure 4b). An exponential fit of the lifetime for the 650 nm phosphorescence emission gives a 1/e time of 56 ± 4 ns, which

dx.doi.org/10.1021/ja306162g | J. Am. Chem. Soc. 2012, 134, 17104−17116

$$[Ru(bpy(CO_2Me)_2)_3]^{2+} \xrightarrow{h\nu} [Ru(bpy(CO_2Me)_2)_3]^{2+*} \quad (1)$$

$$[Ru(bpy(CO_2Me)_2)_3]^{2+*} + S_2O_8^{2-} \longrightarrow [Ru(bpy(CO_2Me)_2)_3]^{3+} + \cdot SO_4^{-} + SO_4^{2-} \quad (2)$$

$$[Ru(bpy(CO_2Me)_2)_3]^{3+} + \mathbf{PV3\_SO3\_SO3}^{2-} \longrightarrow [Ru(bpy(CO_2Me)_2)_3]^{2+} + \cdot\mathbf{PV3\_SO3\_SO3}^{-} \quad (3)$$

$$[Ru(bpy(CO_2Me)_2)_3]^{2+} + \cdot SO_4^{-} \longrightarrow [Ru(bpy(CO_2Me)_2)_3]^{3+} + SO_4^{2-} \quad (4)$$

Figure 5. Proposed elementary steps involved in the generation and decay of PV3 radicals after photosensitization by $[Ru(bpy(CO_2Me))_3]^{2+}$.

is consistent with a bimolecular quenching process between $[Ru(bpy(CO_2Me)_2)_3]^{2+*}$ and $S_2O_8^{2-}$ with a lower limit of $k = 3.6 \times 10^7$ L mol^{-1} s^{-1} (lower limit because of consumption of $S_2O_8^{2-}$ during the photolysis).

These results are satisfactorily explained by the elementary steps summarized in Figure 5. After quenching by the electron-acceptor $S_2O_8^{2-}$ at near diffusion-controlled rates, the $[Ru(bpy(CO_2Me)_2)_3]^{3+}$ thus formed injects a hole into **Na_2PV3_SO3_SO3** resulting in growth of the radical cation absorption with a 4.5 μs time constant. Subsequent degradation of the PV3 radical by excimer formation or other processes leads to the gradual decay of the transient absorption signal. The transient absorption spectrum, shown in Figure 6a,

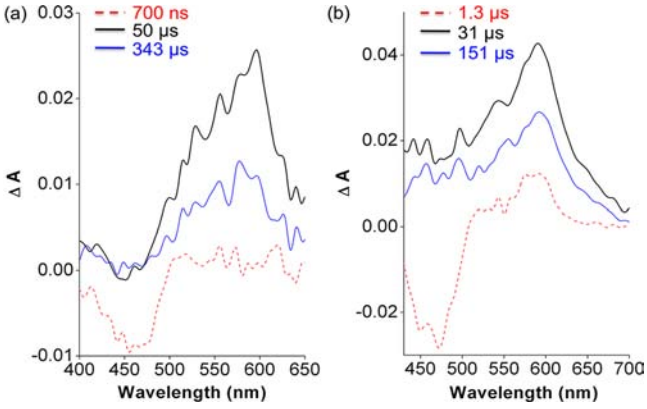

Figure 6. (a) Time evolution of transient absorption spectra of radical cation of **Na_2PV3_SO3_SO3** with vibronic structure. Excitation of $[Ru(bpy(CO_2Me)_2)_3]^{2+}$ at 450 nm. (b) Transient absorption spectra of radical cation of **Cs_2PV3_O3N_2SO3**.

confirms the assignment of the 600 nm signal as the λ_{max} of a PV3 radical cation. The absorption profile is in good agreement with PV3 radical cation reported in tetrahydrofuran solvent.[7] It is interesting to note that the transient absorption spectrum shows the characteristic vibronic fine structure with a frequency of about 690 cm^{-1}. However, due to formation of the strongly oxidizing SO_4^{-} radical when persulfate is used as the sacrificial quencher, **Na_2PV3_SO3_SO3** is rapidly degraded in solution. Therefore, time-resolved measurements had to be conducted with optimized concentrations of the molecular wire and just a few laser shots before replacing the sample. The static UV–visible spectra before and after the laser photolysis experiments clearly demonstrate significant loss of the π–π^* band below 400 nm (Figure S3). To avoid this problem and the complications that arose for the kinetic treatment, an alternative electron acceptor $[Co(NH_3)_5Cl]^{2+}$ was used for the majority of the remaining experiments.

The reduced aquated Co^{II} ions generated by quenching of $[Ru(bpy(CO_2Me)_2)_3]^{2+*}$ by $[Co(NH_3)_5Cl]^{2+}$ cannot be reoxidized to Co^{III} by the radical cation (Table 2). Therefore, spontaneous secondary redox reactions following the electron transfer step do not occur. To probe if the alkyl groups of the multidentate anchors will adversely affect the hole injection kinetics due to oxidative degradation, **Cs_2PV3_O3N_2SO3** was examined in time-resolved optical spectroscopic studies. $[Ru(bpy(CO_2Me)_2)_3]^{2+*}$ is quenched with a lifetime of 81 ± 2 ns, and the radical cation absorption at 600 nm grows with a time constant of 25.8 ± 0.4 μs (Figure 4d). The latter agrees well with the bleach recovery of the sensitizer of 27.7 ± 0.4 μs monitored at 470 nm (Figure 4f). The corresponding average bimolecular hole transfer constant is 7.5×10^8 L mol^{-1} s^{-1}. The cation subsequently decays with a time constant of 343 ± 3 μs; the characteristic transient absorption spectrum is shown in Figure 6b. The chemical stability of the PV3 (**Cs_2PV3_O3N_2SO3**) wire molecule is much higher with $[Co(NH_3)_5Cl]^{2+}$ as the sacrificial acceptor compared to the experiments with $S_2O_8^{2-}$, as can be seen from the negligible loss of UV band intensity below 400 nm after irradiation (Figure S3, experiment with similar concentration and number of laser shots as **Na_2PV3_SO3_SO3** measurements). The electron acceptor $[Co(NH_3)_5Cl]^{2+}$ has a lower aqueous solubility than $S_2O_8^{2-}$, slightly slower quenching rates possibly due to electrostatic repulsion with $[Ru(bpy(CO_2Me))_3]^{2+}$, and substantial UV–visible absorption intensity that limits the usable concentration due to the optical inner filter effect. Despite these limitations, the better stability of the PV3 derivatives in the presence of $[Co(NH_3)_5Cl]^{2+}$ made the Co complex the preferred sacrificial quencher in subsequent transient optical measurements of hole injection into molecular wires anchored on metal oxide surfaces.

2.3. Covalent Attachment of *p*-Oligo(phenylenevinylene) on SiO_2 and Co_3O_4 Nanoparticles.

Inspired by postsynthetic bioconjugation protocols on silica surfaces,[46–52] we sought a procedure that would be suitable for covalent attachment of PV3 wire molecules on SiO_2 and Co_3O_4 nanoparticle surfaces. In initial attempts, peptide coupling condensation reagents[25,26] to form covalent linkages between surface Si–OH or Co–OH groups and the carboxylates from the PV3 wires were employed. For example, **Cs_3PV3_CO2_2SO3** was activated with HCTU as the dehydrating agent prior to adding 12 nm SiO_2 nanoparticles to the aqueous solution, which resulted in a maximum of 8 mol % PV3 surface coverage. After repeated centrifugation and rinsing cycles to remove physisorbed PV3 molecules, the functionalized **SiO_2_PV3_CO2_2SO3** was isolated as a pale yellow, fluorescent solid. FT-IR spectra of a powder of SiO_2 particles with attached PV3 molecules mixed with KBr are shown in Figure 7. After subtracting the spectrum of plain SiO_2 particles (Figure 7b) from the **SiO2_PV3** spectrum (Figure 7a), the resulting difference spectrum (Figure 7c) shows characteristic bands of **Cs_3PV3_CO2_2SO3**. Figure 7d presents the infrared spectrum of solid **Cs_3PV3_CO2_2SO3** in KBr.[49,53] There is good agreement between the spectra of

dx.doi.org/10.1021/ja306162g | J. Am. Chem. Soc. 2012, 134, 17104–17116

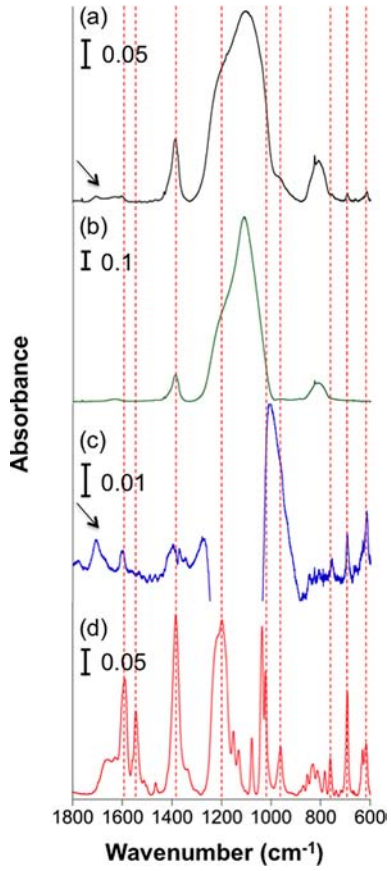

Figure 7. FT-IR spectra of **PV3_CO2_2SO3** molecules anchored on 12 nm SiO_2 nanoparticles. (a) Spectrum of **SiO_2_PV3_CO2_2SO3** in a KBr pellet. (b) Spectrum of SiO_2 nanoparticles in a KBr. (c) Difference spectrum of **SiO_2_PV3_CO2_2SO3** and SiO_2. The black arrow indicates the C═O stretch of anchored silyl ester. (d) Spectrum of **Cs_3PV3_CO2_2SO3** in a KBr. Strong IR bands of **Cs_3PV3_CO2_2SO3** are indicated by dashed lines for convenience.

the neat wire and the anchored wire molecule except for small frequency shifts and broadening of some bands in the case of the anchored molecule. The most significant change is the replacement of the C═O stretch of the carboxylic acid group around 1663 cm^{-1} for pristine **Cs_3PV3_CO2_2SO3** (Figure 7d) by an ester C═O stretch at 1710 cm^{-1} upon covalent anchoring (arrow, Figure 7c).[54] Transmission electron microscopy confirms that the silica nanoparticles remain well dispersed with the original size distribution, although some aggregates exist (Figure S4).

In pursuit of an even simpler protocol to anchor the PV3 wires to metal oxide surfaces, an alternative method that exploits covalent attachment via dehydration was developed. Since multidentate photosensitizers have been successfully adsorbed on TiO_2 surfaces,[4,11−20,55−58] the poly alcohol derivatives **CsPV3_tripod_SO3**, **Cs_2PV3_O3N_2SO3** and **Cs_2PV3_tripod_2SO3** were used to ensure a perpendicular orientation of the wires while enhancing chemical stability through the chelating effect of three anchor points. Briefly, after dispersing the finely crushed PV3 salts with the 12 nm SiO_2 particles in a polar aprotic solvent with a moderate boiling point such as 1,2-dimethoxyethane (DME) and 1,2-difluorobenzene, the reaction mixture was heated to reflux, capped with a Soxhlet extractor containing CaH_2 to dehydrate the solvent. The dehydration is driven to completion by removal of the water byproduct. Excessively high temperatures were avoided to prevent decomposition of the PV3 side-chains and aggregation of the SiO_2 particles by condensation reactions between surface silanol groups of different silica particles. Addition of about 20 mol % of lithium dodecylsulfate as a co-surfactant improved the loading, probably by dispersing the SiO_2 particles. After centrifugation and an aqueous workup procedure similar to the method mentioned before, the functionalized silica material was characterized with vibrational and optical spectroscopy and found to contain the expected spectral features of PV3 wires (Supporting Information Figure S5). The FT-Raman spectrum of **SiO_2_PV3_tripod_2SO3** shown in Figure 8a further corroborates the attachment of

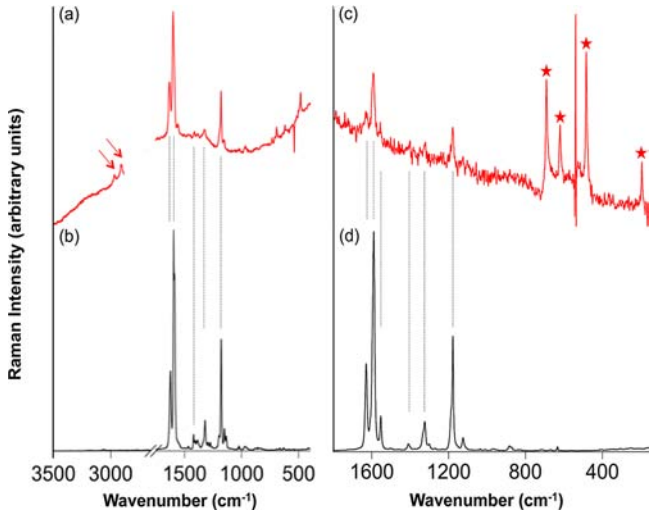

Figure 8. FT-Raman spectra of **PV3_tripod_2SO3** molecules on 12 nm SiO_2 nanoparticles and **PV3_tripod_SO3** molecules on 5 nm Co_3O_4 nanoparticles. (a) Spectrum of powder of **SiO_2_PV3_tripod_2SO3**. The two red arrows indicate Raman bands attributed to C−H stretch modes of methylene groups of the anchored tripod. (b) Spectrum of **Cs_2PV3_tripod_2SO3**. (c) Spectrum of **Co_3O_4_PV3_tripod_SO3**. (d) Spectrum of **CsPV3_tripod_SO3**. Strong Raman bands of the wire molecules are indicated by dashed lines for convenience. Bands with red asterisks originate from Co_3O_4. The sharp spike at 600 cm^{-1} in traces (a) and (c) is due to an instrumental artifact.

intact PV3 wires since all bands of the wire molecule (trace b) appear in the spectrum of the SiO_2 anchored molecule (trace a). Moreover, the C−H stretch absorptions of the tripodal anchor at 2911 and 2868 cm^{-1} are observed with enhanced intensity compared to the free molecule, as was previously noted in the case of tripodal anchoring on another oxide surface (TiO_2). This observation further confirms that **PV3_tripod_2SO3** is attached to the solid oxide surface via the three alcohol groups.[20,49,53,59]

The method using HCTU proved equally effective under the same experimental conditions for the covalent anchoring of PV3 molecules on Co_3O_4 catalyst nanoparticles surfaces. Figure 9 shows FT-IR spectra of **PV3_tripod_SO3** wire molecules anchored on 5 nm Co_3O_4 particles. When subtracting the spectrum of plain 5 nm Co_3O_4 particles (Figure 9b) from the **Co_3O_4_PV3** spectrum (Figure 9a), the resulting difference spectrum (Figure 9c) shows characteristic bands of **CsPV3_tripod_SO3**. Figure 9d presents the infrared spectrum of solid **CsPV3_tripod_SO3** in KBr. There is good agreement between the spectra of the pristine wire and the anchored wire molecule

dx.doi.org/10.1021/ja306162g | J. Am. Chem. Soc. 2012, 134, 17104−17116

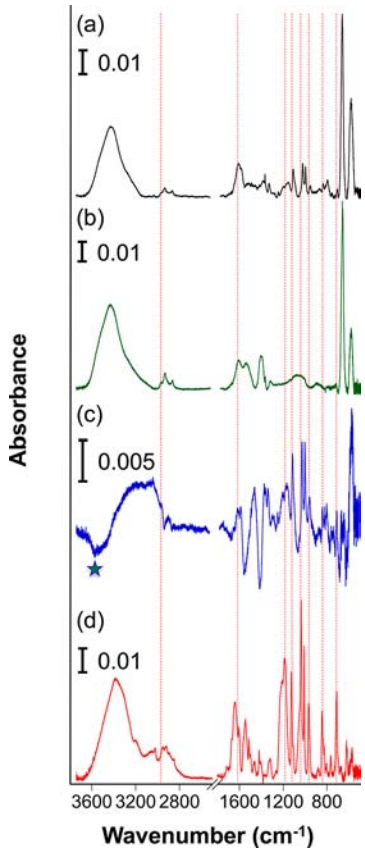

Figure 9. FT-IR spectra of **PV3_tripod_SO3** molecules anchored on 5 nm Co_3O_4 nanoparticles. (a) FT-IR spectrum of **Co_3O_4_PV3_tripod_SO3** in a KBr. (b) FT-IR spectrum of 5 nm Co_3O_4 nanoparticles in a KBr. (c) Difference spectrum of **Co_3O_4_PV3_tripod_SO3** and 5 nm Co_3O_4 (normalized to the Co−O band at 665 cm^{-1}). Strong IR bands of **CsPV3_tripod_SO3**, are indicated by vertical lines for convenience. (d) FT-IR spectrum of **CsPV3_tripod_SO3** in a KBr pellet.

except for small frequency shifts and broadening of some bands in the case of the anchored molecule. Comparison of the FT-Raman spectra of anchored **Co_3O_4_PV3_tripod_SO3** and neat **PV3_tripod_SO3** powder (Figure 8c,d) confirms that the wire molecules remain intact after anchoring. We conclude that this synthetic method provides a general, straightforward protocol for attachment of molecular wires on metal oxide surfaces.

2.4. Kinetics of Hole Injection into *p*-Oligo(phenylenevinylene) Wires Attached to SiO_2 Nanoparticles.

The UV−visible spectrum of **SiO_2_PV3_CO2_2SO3** dispersed in water in the presence of 200 mM Li_2SO_4 is illustrated in the Supporting Information Figure S6. The silica constructs aggregate upon drying and scatter light significantly when redispersed in aqueous solutions. The high concentration of Li^+ aids in the dispersion of the silica constructs, presumably by electrostatically adhering to the negatively charged silica surface under neutral aqueous conditions. Moreover, the Li^+ ions also minimizes adsorption of $[Ru(bpy(CO_2Me)_2)_3]^{2+}$ on the silica surface, thus minimizing triplet energy transfer from MLCT excited $[Ru(bpy(CO_2Me)_2)_3]^{2+}$ to PV3 prior to electron transfer to the acceptor molecules. The Li^+ thus serves to enhance the formation of $[Ru(bpy(CO_2Me)_2)_3]^{3+}$ and subsequent hole transfer to PV3 wire molecules. Assuming that the extinction coefficient of the PV3 moiety remains unchanged after attachment on SiO_2 and taking into account the 200 m^2 g^{-1}surface area of the commercial 12 nm particles, the surface concentration is estimated to be 0.051 PV3 molecules per nm^2 of silica, corresponding to about 22 PV3 molecules per nanoparticle. The optical and photophysical data of free and surface attached PV3 molecules are summarized in Table 3.

Nanosecond optical spectroscopy of **SiO_2_PV3_O3N_2SO3** sample in 250 mM Li^+ aqueous solutions probed at 600 nm gave a rise time of the radical cation of 18 ± 2 μs (Figure 10a) and a decay time of 208 ± 4 μs (Figure 10b). On the basis of a SiO_2 particle concentration of 1.5 × 10^{-6} M, a diffusion controlled bimolecular hole transfer constant of 3.6 × 10^{10} M^{-1} s^{-1} is calculated. Contribution to the signal from any free PV3 molecules detached from the silica particle surface is very small as illustrated in Figure 10a by the trace (gray color) measured for the supernatant solution after sonication and removing the **SiO_2_PV3_O3N_2SO3** particles by centrifugation. Furthermore, control sensitization experiments of free PV3 molecules in the presence and absence of Li^+ (250 mM) confirmed that Li^+ does not affect the hole transfer kinetics within uncertainties (Figure S7). The recovery of the $[Ru(bpy(CO_2Me)_2)_3]^{2+}$ bleach at 470 nm fits an exponential function with a time constant of 16 ± 1 μs (Figure 10c), in agreement with the growth kinetics of the PV3 radical cation. The identity of the PV3 radical cation is confirmed by the transient absorption spectrum shown in Figure 10d. We conclude that hole transfer from the oxidized Ru sensitizer to the anchored PV3 wire molecule is very efficient at a driving force (overpotential) of 480 mV. The inset of Figure 10a shows on an expanded scale the quenching of the $[Ru(bpy(CO_2Me)_2)_3]^{2+*}$ emission by electron transfer to the $[Co(NH_3)_5Cl]^{2+}$ acceptor with a time

Table 3. Photophysical Properties in Aqueous Solutions of Selected PV3 Derivatives and 12 nm Silica Nanoparticles with PV3 Wires Anchored on the Surface

sample	Na_2PV3_SO3_SO3	Cs_2PV3_O3N_2SO3	SiO_2_PV3_CO2_2SO3	SiO_2_PV3_O3N_2SO3	Co_3O_4_PV3_tripod_SO3
λ_{max} (nm)	349	361	324	350	365
ε (10^4 M^{-1} cm^{-1})	4.1	8.0	5.1	8.0	3.7
Surface Coverage (molecules nm^{-2})			0.051	0.097	8.3
Surface Coverage (per nanoparticle)			22	42	417
PV3 Formation τ (μs)	4.5 ± 0.2 (600 nm) 4.9 ± 0.1 (470 nm)	25.8 ± 0.4 (600 nm) 27.7 ± 0.4 (470 nm)	25 ± 8 (600 nm) 30 ± 2 (470 nm)	18 ± 2 (600 nm) 16 ± 1 (470 nm)	10.4 ± 0.2 (470 nm)[a]
PV3 Formation k (10^9 $M^{-1}s^{-1}$)	0.82	0.75	>0.51	36	−[a]

[a]No PV3 radical cation observed on the 10 ns and longer time scale, only recovery of Ru^{II} at 470 nm is detected.

dx.doi.org/10.1021/ja306162g | J. Am. Chem. Soc. 2012, 134, 17104−17116

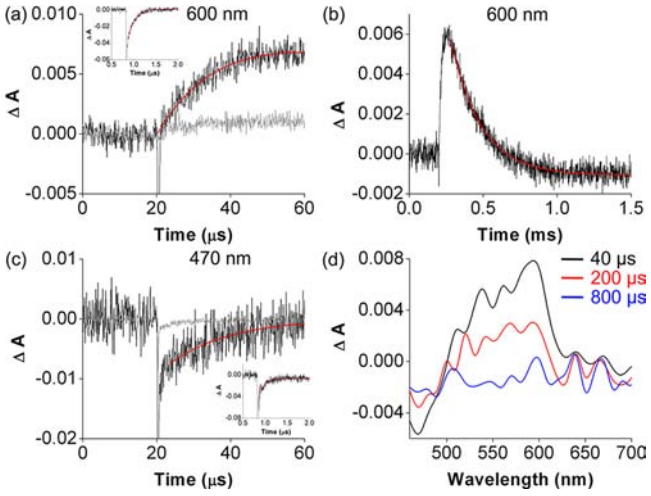

Figure 10. (a) Transient absorption signal at 600 nm upon 450 nm excitation of sensitizer in the presence of **SiO_2_PV3_O3N_2SO3** (4 mg) in a 2 mL suspension ($Co(NH_3)_5Cl_3$, 10 mM; $[Ru(bpy\text{-}(CO_2Me)_2)_3]^{2+}$, 10 μM). The gray trace is the time-resolved signal of the supernatant. Inset: Sensitizer phosphorescence recovery at 600 nm with a lifetime of 160 ± 2 ns. (b) Decay of **SiO_2_PV3_O3N_2SO3** radical cation at 600 nm. (c) Bleach recovery of $[Ru(bpy\text{-}(CO_2Me)_2)_3]^{2+}$ at 470 nm after hole injection into **SiO_2_PV3_O3N_2SO3**. The gray trace is the time-resolved signal of the supernatant. Inset: Bleach recovery at 470 nm with a lifetime of 151 ± 6 ns. (d) Transient absorption spectral decay of **SiO_2_PV3_O3N_2SO3** radical cation after excitation at 450 nm.

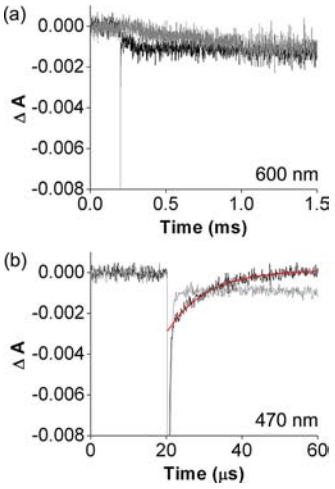

Figure 11. (a) Transient absorption trace (black) at 600 nm upon 450 nm excitation of sensitizer in the presence of **Co_3O_4_PV3_tripod_SO3** ($Co(NH_3)_5Cl_3$, 15 mM; $[Ru(bpy\text{-}(CO_2Me)_2)_3]^{2+}$, 20 μM; Li^+, 0.25 M; CH_3CN:H_2O = 1/5). Gray trace shows transient observed for supernatant. (b) Black trace: Bleach recovery of $[Ru(bpy(CO_2Me)_2)_3]^{2+}$ at 470 nm. The gray trace shows transient observed for supernatant.

constant of 160 ± 2 ns ($k = 6.3 \times 10^8$ M^{-1} s^{-1}). These results indicate that rise and decay of the radical cation generated by hole injection into SiO_2-anchored wire molecules is similar to that observed for the corresponding free **PV3_O3N_2SO3** molecules.

A similar study of time-resolved hole injection was conducted for PV3 molecules anchored on the SiO_2 particle surface by a carboxylate group (**SiO_2_PV3_CO2_2SO3**). The results, presented in Table 3 and Figure S8 are again the same as for the free wire in solution, thus, confirming that anchoring of PV3 wire molecules on an inert oxide surface, whether through a carboxylate group or via a combination of two alcohols plus an amide group, does not substantially affect the fate of the injected hole.

2.5. Hole Injection into *p*-Oligo(phenylenevinylene) Wires Attached to Co_3O_4 Nanocatalyst Particles. When exploring hole injection into PV3 wire molecules covalently attached to Co_3O_4 nanocatalyst particles using $[Ru(bpy\text{-}(CO_2Me)_2)_3]^{2+}$ as the sensitizer and $[Co(NH_3)_5Cl]^{2+}$ as the acceptor (pH 7), no significant absorption of the radical cation was detected at 600 nm on the time scale of nanoseconds and microseconds. Twenty percent acetonitrile was added to the aqueous solution in order to prevent precipitation of the **Co_3O_4_PV3** particles at the desired concentrations. For nanosecond pump−probe measurements with **Co_3O_4_PV3** particles, samples were purged with N_2 in 10 × 2 mm cuvettes and excited at 450 nm (20−30 mJ/pulse). The higher power and shorter path length for the probe light compared to the **SiO_2_PV3** study were necessary to provide sufficient signal-to-noise due to light absorption by the black-colored Co_3O_4 nanoparticles. Figure 11a shows the transient response at 600 nm for a **Co_3O_4_PV3_tripod_SO3** sample in 250 mM Li^+ monitored under concentration conditions similar to those of **SiO_2_PV3** (Co_3O_4 particle concentration 0.46 μM), but with substantially higher concentration of attached PV3 wire molecules for **Co_3O_4_PV3_tripod_SO3**: 417 **PV3_tripod_-SO3** molecules per Co_3O_4 particles versus 22 **PV3−O3N** molecules per SiO_2 particle. Yet, no significant $PV3^+$ radical cation signal can be discerned from the 600 nm transient absorption experiment; only the emission of $[Ru(bpy\text{-}(CO_2Me)_2)_3]^{2+*}$ and its decay by conversion to $[Ru(bpy\text{-}(CO_2Me)_2)_3]^{3+}$ is observed. By contrast, bleach recovery of $[Ru(bpy(CO_2Me)_2)_3]^{2+}$ with a time constant of 10.4 ± 0.2 μs can clearly be seen from Figure 11b, indicating hole injection into anchored PV3 molecules. The same observations were made for Co_3O_4−PV3 samples with lower PV3 loading. No significant recovery of the bleach at 470 nm is detected on the tens of μs time scale when conducting the sensitization experiments with bare (wire-free) Co_3O_4 particles (the hole injection time from $[Ru(bpy(CO_2Me)_2)_3]^{3+}$ into Co_3O_4 particles has been measured as 25 ms).[60] Contributions to the signal from any free PV3 molecules detached from the Co_3O_4 particle surface are absent, as can be seen in Figure 11 by the faint traces of photolysis experiments with supernatant solutions recorded under the same conditions used for the **Co_3O_4_PV3_tripod_SO3** suspensions. We conclude that hole injection from $[Ru(bpy(CO_2Me)_2)_3]^{3+}$ to PV3 wire molecules attached to Co_3O_4 molecules occurs, yet no concurrent radical cation signal on the time scale of tens of nanoseconds or microseconds is observed.

3. DISCUSSION

p-Oligo(phenylenevinylene) molecules with 3 units (PV3) offer suitable prototypes as hole conducting molecular wires with reasonable photochemical stability for charge transport from a visible light sensitizer to a Co_3O_4 nanoparticle catalyst for water oxidation. We have synthesized a small library of PV3 derivatives for the covalent anchoring of the wire molecules on the oxide particle surface that includes anchoring groups such as tripodal $-C(=O)NHC(CH_2OH)_3$ or bidentate $-C(=O)N(CH_2CH_2OH)_2$. Sulfonate groups in ortho and/or para position on the opposite end of the wire molecule

dx.doi.org/10.1021/ja306162g | J. Am. Chem. Soc. 2012, 134, 17104−17116

facilitate radial arrangement of the wire molecules and at the same time afford adequate water solubility for spectroscopic characterization and hole injection experiments. Anchoring of PV3 wire molecules on Co_3O_4 nanoparticle catalyst surfaces, and on insulating SiO_2 for control experiments using either HCTU coupling or the Soxhlet extractor dehydration method, was found to provide stable surface attachment for spectroscopic studies and photosensitized charge injection experiments in aqueous solution. These anchors are known to impose radial (vertical) orientation of the wire molecule according to previous work by Meyer and Gallopini in the case of TiO_2 surfaces,[11,16−20] thus enforcing proper geometry of the wire molecules in addition to electrostatic repulsion between the negatively charge Co_3O_4 surface and the sulfonate groups.

With covalent attachment of intact wire molecules to insulating SiO_2 and catalytic Co_3O_4 nanoparticle surfaces established by FT-Raman, FT-IR and UV−visible spectroscopy, time-resolved optical absorption measurements reveal efficient hole injection from the oxidized sensitizer into the anchored wire molecules. While hole transfer from oxidized sensitizer into PV3 wires attached to SiO_2 nanoparticles is observed both by the growth of the 600 nm transient absorption of the $PV3^+$ radical cation and the recovery of the reduced Ru sensitizer at 470 nm, the absence of a signal at 600 nm for wires attached to Co_3O_4 indicates a much shorter residence time of the hole on PV3 attached to these catalyst particles. Comparison of the transient signal amplitude at 600 nm for PV3 on SiO_2 particles (Figure 10a) and the noise of the kinetic trace for PV3 on Co_3O_4 at the same wavelength (Figure 11a) allows us to estimate an upper limit for the hole residence time in the case of Co_3O_4−PV3. For SiO_2−PV3, the buildup of $PV3^+$ absorbance is 0.007 with negligible decay on the time scale of its 18 μs rise. In the case of Co_3O_4−PV3, the 1/e time for $PV3^+$ growth is 10.4 μs ($1/k_1$) as inferred from the rate of 470 nm recovery of the reduced sensitizer. Buildup of intensity at 600 nm (noise 0.0008 absorbance units) is prevented by a fast decay process of $PV3^+$. From these observations, we calculate that $PV3^+$ is depleted at a rate of $k_2 = 7 \times 10^5\ s^{-1}$ or larger (k_2 calculated according to $0.0008/0.007 = 1 - k_2/(k_2 + k_1)$, with $k_1 = 9.6 \times 10^4\ s^{-1}$).

The most probable pathway of $PV3^+$ loss is hole transfer to the attached Co_3O_4 particle. Alternative hole transfer pathways, in particular reaction with other wire molecules or unknown species, are very unlikely because of the observed long hole lifetime, under otherwise similar experimental conditions, for wire molecules anchored on (insulating) SiO_2 particles. The fast hole injection from anchored PV3 to Co_3O_4 is plausible in particular because the HOMO of the wire molecule (1.4 V)[6] is energetically well aligned with the HOMO of the Co_3O_4 acceptor particle (1.2 V). While we are not aware of precedents for hole transport across conducting wire molecules covalently attached to a metal oxide surface, hole transfer by an incoherent hopping mechanism on submicrosecond time scales was reported for organic donor−acceptor systems featuring oligo(phenylenevinylene) bridges.[6,7,18,55,61−65] The fastest reported hole transfer so far from a visible light sensitizer, a $Ru(bpy)_3$ congener attached to a metal oxide nanoparticle catalyst, IrO_2, via an acetylacetonate anchor was determined by Mallouk to be 2.2 ms.[4,5] We conclude that coupling of a sensitizer with Co_3O_4 particles via oligo-para(phenylenevinylene) molecular wire may offer a new approach for efficient light-induced hole transfer to a catalyst nanoparticle.

4. CONCLUSIONS

Hole conducting wire molecules of type 1,3-di((*E*)-styryl)-benzene were functionalized with carboxylate, or with bi- or tridentate polyalcohol amide anchors for covalent attachment to Co_3O_4 and SiO_2 nanoparticle surfaces with a preferential radial arrangement. No drastic change of HOMO and LUMO energy levels by the functionalization was noted as indicated by the UV−vis spectra and the fact that hole transfer from $[Ru(bpy(CO_2Me)_2)_3]^{3+}$ to anchored wire molecules was observed for all derivatives. Two methods were developed for anchoring of the wire molecules. The first uses a peptide coupling agent (HCTU) for activating the OH groups while the other is a more general method for driving condensation of the OH anchor groups of PV3 with surface hydroxyl groups to completion using dehydration by CaH_2. FT-infrared and FT-Raman signatures present spectroscopic evidence for covalent surface attachment.

Observation of the PV3 radical cation by transient optical absorption spectroscopy, upon excitation of $Ru(bpy(CO_2Me)_2)_3$ in the presence of an electron acceptor in homogeneous aqueous solution, provides direct evidence for hole injection into wire molecules. The same radical cation signal with similar kinetics (10−20 μs growth, hundreds of μs decay) is observed for wire molecules attached to SiO_2 nanoparticles. The growth kinetics of $PV3^+$, which is mirrored by the recovery of reduced $Ru(bpy(CO_2Me)_2)_3$ sensitizer, indicates very efficient charge transfer into free wire molecules as well as those anchored on the silica surface. For PV3 anchored on Co_3O_4 catalyst particles, no radical cation signal is observed despite the fact that hole injection into wire molecules is indicated by fast (10.4 μs) recovery of reduced $Ru(bpy(CO_2Me)_2)_3$ sensitizer. This observation implies that the hole is transferred from the wire to the Co_3O_4 particle within a microsecond or faster. This is consistent with the favorable energy alignment of the HOMO of wire and catalyst. Hence, the approach of using anchored wire molecules may open up an efficient hole transfer pathway from oxidized donor $[Ru(bpy(CO_2Me)_2)_3]^{3+}$ to Co_3O_4 catalyst particles. In the next step, casting of a dense phase, few nanometer thin silica layer around the wire molecules will introduce a physical barrier for separating the water oxidation catalysis from the light absorber and the reductive chemistry.[66] At the same time, the surrounding silica protects the wire molecules from oxidative damage. When implemented in the form of asymmetrically functionalized core−shell nanotubes instead of the spherical core−shell particles, separate physical spaces will be available for O_2 evolution and light absorber/reduction chemistry. Separation of the two half reactions by a physical barrier is a critical ingredient of an artificial photosynthetic system.

5. EXPERIMENTAL SECTION

5.1. Synthetic Materials and Methods. Silica gel (SiliaFlash P60, SiliCycle) was used for column chromatography, while analytical thin layer chromatography was performed using EMD Chemicals, Inc. 60 F_{254} silica gel (precoated plastic sheets, 0.25 mm thick). All moisture-sensitive reactions were performed using Schlenk techniques under a nitrogen atmosphere. Deuterated solvents and isotopically labeled reagents were procured from Cambridge Isotope Laboratories (Cambridge, MA). Solvents such as acetonitrile, chloroform, dichloromethane, ethyl acetate, hexanes, and toluene were obtained from EMD Chemicals, Inc. or Honeywell and used without further purification. All other chemicals, including anhydrous DMF and THF, were purchased from Sigma-Aldrich (St. Louis, MO) and were used as

received. Details for the synthesis of functionalized PV3 molecular wires are presented in the Supporting Information.

5.2. Instrumentation. ^{1}H and ^{13}C NMR spectra were recorded using a Bruker Biospin Avance II 500 MHz High Performance NMR Spectrometer in the Chemistry NMR Facility at the Molecular Foundry Organic and Macromolecular Synthesis Facility, LBNL. The NMR chemical shifts are reported in the standard δ notation of parts per million (ppm) with respect to residual protonated solvent; coupling constants are reported in Hz. High-resolution mass spectral analyses were performed by the QB3/Mass Spectrometry facility at the College of Chemistry, University of California, Berkeley. UV−visible absorption spectra and kinetic runs were recorded using a Shimadzu UV-2100 spectrophotometer, with solution samples in 10 mm × 5 mm or 10 mm × 2 mm cuvettes. FT-IR spectra were recorded at 0.5 cm^{-1} resolution using a Bruker IFS88 or IFS66V spectrophotometer equipped with liquid nitrogen cooled MCT detectors. FT-Raman spectra were recorded with the IFS66V spectrophotometer with a FT-Raman module FRA-106 at 1 cm^{-1} resolution.

5.3. Time-Resolved Optical Absorption Spectroscopy. For the nanosecond optical kinetics measurements, an Edinburgh Instruments model LP920 transient absorption spectrometer equipped with a pulsed Xe probe lamp or a CW halogen lamp (for measurements >1 ms) was used in conjunction with a Nd:YAG laser-pumped tunable Optical Parametric Oscillator (Continuum model Surelite II and Surelite OPO Plus) as the excitation source. The laser pulse width was 8 ns and the repetition rate was 10 Hz. For measurements of the silica nanoparticle constructs, transient absorption spectroscopy for lifetimes shorter than 20 ns is complicated by visible light scattering of the incident pulse and emission from defect sites of the silica material.

In typical nanosecond pump−probe measurements, samples of the dissolved PV3 and silica constructs in sealed 10 × 5 mm cuvettes are purged with N_2 and illuminated with 450 nm laser pulses at 3−8 mJ for kinetics measurements, and up to 22 mJ pulse energy when recording transient absorption spectral maps. The laser excitation beam was at right angle to the Xe (or halogen lamp) probe beam. For samples of the Co_3O_4 constructs, sealed 10 × 2 mm cuvettes containing the nanoparticulate suspension are purged with N_2 and illuminated with 450 nm laser pulses at 20−30 mJ for kinetics measurements. A colinear geometry of the laser excitation beam and the Xe probe beam was adopted to maximize the overlap of the two beams. The wavelength of 450 nm was used to excite the MLCT transition of $[Ru(bpy(CO_2Me))_3]^{2+}$ while avoiding direct excitation of the PV3 molecules. A large excess of the sacrificial electron acceptors $S_2O_8^{2-}$ or $Co(NH_3)_5Cl_3$ was used to ensure a large quantum efficiency for generating $[Ru(bpy(CO_2Me))_3]^{3+}$. To obtain the time constants for the elementary steps, the data were fit to single exponential or biexponential functions:

$$y = y_0 + A_1\, e^{(t-\tau_0)/\tau_1}$$

$$y = y_0 + A_1\, e^{(t-\tau_0)/\tau_1} + A_2\, e^{(t-\tau_0)/\tau_2}$$

The parameters y_0, τ_0, A_n, and τ_n were determined by a least-squares fitting procedure. The term y_0 corresponds to the vertical intercept at infinite time and depends on whether the signal recovers to the baseline or retains a long-term bleach or absorption in the measurement window. The variable τ_0 is the delay time of the excitation pulse after start of the probe measurement. A_n is the change in optical density after irradiation for the nth exponential term, while τ_n is the time constant of the corresponding nth fit. Biexponential fits are used only when two consecutive elementary reactions are anticipated. This is the case for probing at 600 nm where the decay of $[Ru(bpy(CO_2Me))_3]^{2+*}$ phosphorescence is immediately followed by growth of the absorption of PV3 radical cation.

■ ASSOCIATED CONTENT

Ⓢ Supporting Information

Detailed synthesis methods of functionalized PV3 molecular wires. Spectroscopic measurements, time-resolved data, and TEM images on some of the other PV3 derivatives and silica constructs. This material is available free of charge via the Internet at http://pubs.acs.org.

■ AUTHOR INFORMATION

Corresponding Author

HMFrei@lbl.gov

Present Address

[†]Dept. of Chemistry, University of Oxford, South Parks Road, Oxford

Notes

The authors declare no competing financial interest.

■ ACKNOWLEDGMENTS

This work was funded by the Helios Solar Energy Research Center, which is supported by the Director, Office of Science, Office of Basic Energy Sciences of the U.S. Department of Energy under Contract No. DE-AC02-05CH11231. Anil Agiral, Rubicon Postdoctoral Fellow, acknowledges support by The Netherlands Organization for Scientific Research (NWO). Portions of this work (NMR measurements) were performed as a User Project at the Molecular Foundry, Lawrence Berkeley National Laboratory, which is supported by the Office of Science, Office of Basic Energy Sciences, of the U.S. Department of Energy under Contract No. DE-AC02-05CH11231. The authors thank Dr. Beth Anne McClure for assistance with the transient absorption measurements.

■ REFERENCES

(1) Jiao, F.; Frei, H. *Angew. Chem., Int. Ed.* **2009**, *48*, 1841.
(2) Jiao, F.; Frei, H. *Energy Environ. Sci.* **2010**, *3*, 1018.
(3) Fogarty, J. C.; Aktulga, H. M.; Grama, A. Y.; van Duin, A. C. T.; Pandit, S. A. *J. Chem. Phys.* **2010**, *132*, 174704.
(4) Youngblood, W. J.; Lee, S. H. A.; Kobayashi, Y.; Hernandez-Pagan, E. A.; Hoertz, P. G.; Moore, T. A.; Moore, A. L.; Gust, D.; Mallouk, T. E. *J. Am. Chem. Soc.* **2009**, *131*, 926.
(5) Youngblood, W. J.; Lee, S. H.; Maeda, K.; Mallouk, T. E. *Acc. Chem. Res.* **2009**, *42*, 1966.
(6) Davis, W. B.; Svec, W. A.; Ratner, M. A.; Wasielewski, M. R. *Nature* **1998**, *396*, 60.
(7) Davis, W. B.; Ratner, M. A.; Wasielewski, M. R. *Chem. Phys.* **2002**, *281*, 333.
(8) Pavlishchuk, V. V.; Addison, A. W. *Inorg. Chim. Acta* **2000**, *298*, 97.
(9) Kalyanasundaram, K. *Coord. Chem. Rev.* **1982**, *46*, 159.
(10) Grätzel, M. *Acc. Chem. Res.* **2009**, *42*, 1788.
(11) Hoertz, P. G.; Carlisle, R. A.; Meyer, G. J.; Wang, D.; Piotrowiak, P.; Galoppini, E. *Nano Lett.* **2003**, *3*, 325.
(12) Hardin, B. E.; Sellinger, A.; Moehl, T.; Humphry-Baker, R.; Moser, J. E.; Wang, P.; Zakeeruddin, S. M.; Gratzel, M.; McGehee, M. D. *J. Am. Chem. Soc.* **2011**, *133*, 10662.
(13) McNamara, W. R.; Snoeberger, R. C.; Li, G.; Schleicher, J. M.; Cady, C. W.; Poyatos, M.; Schmuttenmaer, C. A.; Crabtree, R. H.; Brudvig, G. W.; Batista, V. S. *J. Am. Chem. Soc.* **2008**, *130*, 14329.
(14) Xiao, D. Q.; Martini, L. A.; Snoeberger, R. C.; Crabtree, R. H.; Batista, V. S. *J. Am. Chem. Soc.* **2011**, *133*, 9014.
(15) Franking, R. A.; Landis, E. C.; Hamers, R. J. *Langmuir* **2009**, *25*, 10676.
(16) Galoppini, E.; Guo, W.; Zhang, W.; Hoertz, P. G.; Qu, P.; Meyer, G. J. *J. Am. Chem. Soc.* **2002**, *124*, 7801.

(17) Galoppini, E.; Guo, W. Z.; Qu, P.; Meyer, G. J. *J. Am. Chem. Soc.* **2001**, *123*, 4342.
(18) Meyer, G. J. *Inorg. Chem.* **2005**, *44*, 6852.
(19) Piotrowiak, P.; Galoppini, E.; Wei, Q.; Meyer, G. J.; Wiewior, R. *J. Am. Chem. Soc.* **2003**, *125*, 5278.
(20) Wang, D.; Mendelsohn, R.; Galoppini, E.; Hoertz, P. G.; Carlisle, R. A.; Meyer, G. J. *J. Phys. Chem. B* **2004**, *108*, 16642.
(21) Garner, L. E.; Park, J.; Dyar, S. M.; Chworos, A.; Sumner, J. J.; Bazan, G. C. *J. Am. Chem. Soc.* **2010**, *132*, 10042.
(22) Nielsen, C. B.; Johnsen, M.; Arnbjerg, J.; Pittelkow, M.; McIlroy, S. P.; Ogilby, P. R.; Jorgensen, M. *J. Org. Chem.* **2005**, *70*, 7065.
(23) Abbel, R.; Grenier, C.; Pouderoijen, M. J.; Stouwdam, J. W.; Leclere, P. E. L. G.; Sijbesma, R. P.; Meijer, E. W.; Schenning, A. P. H. J. *J. Am. Chem. Soc.* **2009**, *131*, 833.
(24) Gaylord, B. S.; Wang, S. J.; Heeger, A. J.; Bazan, G. C. *J. Am. Chem. Soc.* **2001**, *123*, 6417.
(25) Albericio, F. *Curr. Opin. Chem. Biol.* **2004**, *8*, 211.
(26) Albericio, F.; Bofill, J. M.; El-Faham, A.; Kates, S. A. *J. Org. Chem.* **1998**, *63*, 9678.
(27) Ley, S. V.; Stewart-Liddon, A. J. P.; Pears, D.; Perni, R. H.; Treacher, K. *Beilstein J. Org. Chem.* **2006**, *2*, 15.
(28) Sajiki, H.; Hattori, K.; Hirota, K. *J. Org. Chem.* **1998**, *63*, 7990.
(29) Cui, Z.; Zhang, S.; Yang, J.; Tang, L. *Front. Chem. China* **2008**, *3*, 425.
(30) Geng, M.; Zhang, D.; Wu, X.; He, L.; Gong, B. *Org. Lett.* **2009**, *11*, 923.
(31) Reuter, C.; Wienand, W.; Hubner, G. M.; Seel, C.; Vogtle, F. *Chem.—Eur. J.* **1999**, *5*, 2692.
(32) Colaneri, N. F.; Bradley, D. D. C.; Friend, R. H.; Burn, P. L.; Holmes, A. B.; Spangler, C. W. *Phys. Rev. B* **1990**, *42*, 11670.
(33) Meyer, G. J. *Inorg. Chem.* **2005**, *44*, 6852.
(34) Liu, D.; Hug, G. L.; Kamat, P. V. *J. Phys. Chem.* **1995**, *99*, 16768.
(35) Morris, N. D.; Suzuki, M.; Mallouk, T. E. *J. Phys. Chem. A* **2004**, *108*, 9115.
(36) White, H. S.; Becker, W. G.; Bard, A. J. *J. Phys. Chem.* **1984**, *88*, 1840.
(37) Sivasankar, N.; Weare, W. W.; Frei, H. *J. Am. Chem. Soc.* **2011**, *133*, 12976.
(38) Bachmeier, A. Diploma Thesis, Friedrich-Alexander-Universität, Erlangen-Nürnberg, 2010.
(39) Eskelinen, E.; Luukkanen, S.; Haukka, M.; Ahlgren, M.; Pakkanen, T. A. *J. Chem. Soc., Dalton* **2000**, 2745.
(40) Kavarnos, G. J.; Turro, N. J. *Chem. Rev.* **1986**, *86*, 401.
(41) Pavlishchuk, V. V.; Addison, A. W. *Inorg. Chim. Acta* **2000**, *298*, 97.
(42) Schwalbe, M.; Schafer, B.; Gorls, H.; Rau, S.; Tschierlei, S.; Schmitt, M.; Popp, J.; Vaughan, G.; Henry, W.; Vos, J. G. *Eur. J. Inorg. Chem.* **2008**, 3310.
(43) Curtis, N. J.; Lawrance, G. A.; Sargeson, A. M. *Aust. J. Chem.* **1983**, *36*, 1327.
(44) Mills, A.; Valenzuela, M. A. *J. Photochem. Photobiol., A* **2004**, *165*, 25.
(45) Huie, R. E.; Clifton, C. L.; Neta, P. *Radiat. Phys. Chem.* **1991**, *38*, 477.
(46) Gerion, D.; Herberg, J.; Bok, R.; Gjersing, E.; Ramon, E.; Maxwell, R.; Kurhanewicz, J.; Budinger, T. F.; Gray, J. W.; Shuman, M. A.; Chen, F. F. *J. Phys. Chem. C* **2007**, *111*, 12542.
(47) Gerion, D.; Pinaud, F.; Williams, S. C.; Parak, W. J.; Zanchet, D.; Weiss, S.; Alivisatos, A. P. *J. Phys. Chem. B* **2001**, *105*, 8861.
(48) Kumar, R.; Roy, I.; Hulchanskyy, T. Y.; Goswami, L. N.; Bonoiu, A. C.; Bergey, E. J.; Tramposch, K. M.; Maitra, A.; Prasad, P. N. *ACS Nano* **2008**, *2*, 449.
(49) Li, H. Y.; Tripp, C. P. *J. Phys. Chem. B* **2004**, *108*, 18318.
(50) Rossi, L. M.; Shi, L. F.; Quina, F. H.; Rosenzweig, Z. *Langmuir* **2005**, *21*, 4277.
(51) Wang, L.; Zhao, W. J.; Tan, W. H. *Nano Res.* **2008**, *1*, 99.
(52) Xiao, H. N.; Cezar, N. *J. Colloid Interface Sci.* **2003**, *267*, 343.
(53) Saavedra, H. M.; Thompson, C. M.; Hohman, J. N.; Crespi, V. H.; Weiss, P. S. *J. Am. Chem. Soc.* **2009**, *131*, 2252.
(54) Colthup, N. B.; Daly, L. H.; Wiberley, S. E. *Introduction to Infrared and Raman Spectroscopy*, 3rd ed.; Academic Press: New York, 1990; p 301.
(55) Galoppini, E. *Coord. Chem. Rev.* **2004**, *248*, 1283.
(56) Myahkostupov, M.; Piotrowiak, P.; Wang, D.; Galoppini, E. *J. Phys. Chem. C* **2007**, *111*, 2827.
(57) Wei, Q.; Galoppini, E. *Tetrahedron* **2004**, *60*, 8497.
(58) Yi, K. J.; Wang, H.; Lu, Y. F.; Yang, Z. Y. *J. Appl. Phys.* **2007**, 101.
(59) Moskovits, M.; Suh, J. S. *J. Phys. Chem.* **1984**, *88*, 5526.
(60) De Respinis, M. Master Thesis, Technical University of Denmark, Copenhagen, 2011.
(61) Giacalone, F.; Segura, J. L.; Martin, N.; Guldi, D. M. *J. Am. Chem. Soc.* **2004**, *126*, 5340.
(62) Gray, H. B.; Halpern, J. *Proc. Natl. Acad. Sci. U.S.A.* **2005**, *102*, 3533.
(63) Hanss, D.; Walther, M. E.; Wenger, O. S. *Coord. Chem. Rev.* **2010**, *254*, 2584.
(64) Gust, D.; Moore, T. A.; Moore, A. L. *Acc. Chem. Res.* **2009**, *42*, 1890.
(65) Zhao, Y.; Swierk, J. R.; Megiatto, J. D.; Sherman, B.; Youngblood, W. J.; Qin, D.; Lentz, D. M.; Moore, A. L.; Moore, T. A.; Gust, D.; Mallouk, T. E. *Proc. Natl. Acad. Sci. U.S.A.* **2012**, *109*, 15612.
(66) Agiral, A.; Soo, H. S.; Frei, H. *J. Am. Chem. Soc.*, submitted for publication, **2012**.